

Variational Mapping of Chern Bands to Landau Levels: Application to Fractional Chern Insulators in Twisted MoTe₂

Bohao Li¹ and Fengcheng Wu^{1,2,*}

¹*School of Physics and Technology, Wuhan University, Wuhan 430072, China*

²*Wuhan Institute of Quantum Technology, Wuhan 430206, China*

We present a theoretical study of mapping between Chern bands and generalized Landau levels in twisted bilayer MoTe₂, where fractional Chern insulators have been observed. We construct an exact Landau-level representation of moiré bands, where the bases are derived from Landau-level wavefunctions dressed by spinors aligned or antialigned with the layer pseudospin skyrmion field and maintain uniform quantum geometry. We further generalize the dressed zeroth Landau level to a variational wavefunction with an ideal yet nonuniform quantum geometry and variationally maximize its weight in the first moiré band. The variational wavefunction quantitatively reproduces the exact diagonalization spectra of fractional Chern insulators at hole-filling factors $\nu_h = 2/3$ and $3/5$ across a large twist-angle range. Our work introduces a new approach to studying fractional states by bridging the gap between Chern bands and Landau levels.

Introduction.— Fractional Chern insulators (FCIs), originally proposed in theory [1–5] as lattice generalizations of fractional quantum Hall states in Landau levels (LLs), have now been observed in several van der Waals heterostructures [6–12]. Among them, FCIs at zero magnetic field were first realized in twisted bilayer MoTe₂ (*t*MoTe₂) [8–11]. Transport studies of *t*MoTe₂ have identified both integer Chern insulators at $\nu_h = 1$ and FCIs at $\nu_h = 2/3$ and $3/5$ [10, 11], further characterized through the optical spectrum [8, 9], electronic compressibility [9] and real-space local imaging [13, 14]. Moreover, a recent experiment has reported evidence of fractional quantum spin Hall effect in *t*MoTe₂ at $\nu_h = 3$ [15]. While earlier theoretical studies predicted Chern bands [16–18] and FCIs [19–21] in twisted transition metal dichalcogenide homobilayers, these experimental breakthroughs have sparked many further theoretical investigations into the rich quantum phases of matter presented in this system [22–51].

The microscopic mechanism underlying the formation of FCIs remains a fundamental theoretical question in *t*MoTe₂. One approach involves establishing connections between Bloch Chern bands and LLs [52–68]. In *t*MoTe₂, the first moiré valence band has a Chern number $|C| = 1$ and nearly, though not exactly, saturates the trace inequality for quantum geometry at a magic twist angle θ_m , signaling similarities with the zeroth LL (0LL) [23]. Remarkably, the exact-diagonalization (ED) spectra of *t*MoTe₂, with the many-body Hamiltonian projected onto the first band, resembles those of 0LL, aiding in the numerical determination of FCIs at ν_h with odd denominators and composite Fermi liquid at $\nu_h = 1/2$ [22–25]. While connections between topological moiré bands in *t*MoTe₂ and LLs have been made in different approximate limits [39–41], a quantitative mapping strategy in the generic case is still lacking.

In this Letter, we introduce a strategy that begins with an exact LL representation of moiré bands in *t*MoTe₂. The construction relies on the layer pseudospin field,

which forms a skyrmion lattice [16] and generates a non-Abelian gauge field in the local frame [39]. The Bloch bases in this representation consist of *dressed* LL wavefunctions [Eq. (14)] that maintain uniform quantum geometry. The average weight of the first moiré band on the dressed 0LL states is considerable (~ 0.75) but noticeably below unity at θ_m . We then extend the dressed 0LL states to generalized 0LL wavefunctions [Eq. (16)] with an ideal but nonuniform quantum geometry [59] and optimize their weight in the first moiré band using a variational approach, reaching a maximum of 0.95 at θ_m . We further perform ED studies with Coulomb interactions projected onto both the original wavefunction of the first band and the variational wavefunction. Both models consistently yield FCIs at $\nu_h = 2/3$ and $3/5$, with a quantitative agreement in the energy spectra.

Moiré Hamiltonian.— Moiré Hamiltonian for valence states in *t*MoTe₂ at +*K* valley is given by [16, 30],

$$H = \begin{pmatrix} -\frac{\hbar^2(\hat{\mathbf{k}}-\boldsymbol{\kappa}_+)^2}{2m^*} + \Delta_+(\mathbf{r}) & \Delta_t(\mathbf{r}) \\ \Delta_t^\dagger(\mathbf{r}) & -\frac{\hbar^2(\hat{\mathbf{k}}-\boldsymbol{\kappa}_-)^2}{2m^*} + \Delta_-(\mathbf{r}) \end{pmatrix}, \quad (1)$$

where $\hat{\mathbf{k}}$ is the momentum operator, m^* is the effective mass, $\boldsymbol{\kappa}_\pm = \frac{4\pi}{3a_M}(-\frac{\sqrt{3}}{2}, \mp\frac{1}{2})$ are located at corners of moiré Brillouin zone, $a_M \approx a_0/\theta$ is the moiré period, θ is the twist angle, and $a_0 = 3.52 \text{ \AA}$ is the monolayer lattice constant. $\Delta_\pm(\mathbf{r})$ and $\Delta_t(\mathbf{r})$ are given by

$$\begin{aligned} \Delta_\pm(\mathbf{r}) &= 2V_1 \sum_{j=1,3,5} \cos(\mathbf{g}_j^{(1)} \cdot \mathbf{r} \pm \psi) + 2V_2 \sum_{j=1,3,5} \cos(\mathbf{g}_j^{(2)} \cdot \mathbf{r}), \\ \Delta_t(\mathbf{r}) &= w_1(1 + e^{-i\mathbf{g}_2^{(1)} \cdot \mathbf{r}} + e^{-i\mathbf{g}_3^{(1)} \cdot \mathbf{r}}) \\ &\quad + w_2(e^{-i\mathbf{g}_2^{(2)} \cdot \mathbf{r}} + e^{-i\mathbf{g}_1^{(1)} \cdot \mathbf{r}} + e^{-i\mathbf{g}_4^{(1)} \cdot \mathbf{r}}), \end{aligned} \quad (2)$$

where $\mathbf{g}_i^{(1)} = \frac{4\pi}{\sqrt{3}a_M}[\cos \frac{\pi(i-1)}{3}, \sin \frac{\pi(i-1)}{3}]$ and $\mathbf{g}_i^{(2)} = \frac{4\pi}{a_M}[\cos \frac{\pi(2i-1)}{6}, \sin \frac{\pi(2i-1)}{6}]$ are moiré reciprocal lattice vectors. We use model parameters fitted from first-principles band structure at $\theta = 3.89^\circ$ [30],

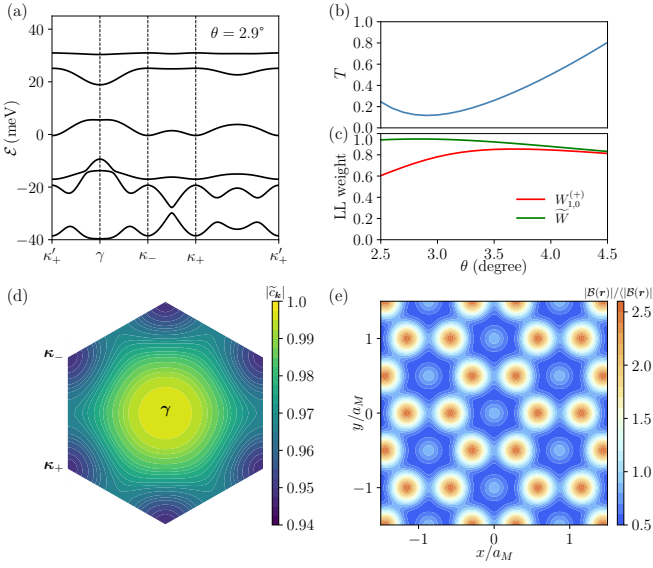


FIG. 1. (a) Moiré band structure of $t\text{MoTe}_2$ at $\theta = 2.9^\circ$. (b) T of the first band as a function of θ . (c) LL weight $W_{1,0}^{(+)}$ (red line) and \tilde{W} (green line) as functions of θ . (d) Overlap $|\tilde{c}_{\mathbf{k}}| = |\langle \varphi_{1,\mathbf{k}} | \Theta_{\mathbf{k}} \rangle|$ in moiré Brillouin zone. (e) Map of $|\mathcal{B}(\mathbf{r})|$ scaled by its spatial average. θ is 2.9° in (d) and (e).

where the effective mass $m^* = 0.62 m_e$ (m_e is the electron rest mass) and $(\psi, V_1, w_1, V_2, w_2) = (-88.43^\circ, 7.94 \text{ meV}, -10.77 \text{ meV}, 20.00 \text{ meV}, 10.21 \text{ meV})$. Here we use this particular set of parameters to illustrate the main physics [25–30].

A representative moiré band structure is shown in Fig. 1(a). We focus on the first moiré valence band with a narrow bandwidth and a Chern number $\mathcal{C} = +1$. The quantum geometry of this band, as characterized by Berry curvature $\Omega_{\mathbf{k}}$ and trace of quantum metric $\text{Tr } g_{\mathbf{k}}$, is illustrated in Fig. 2 for $\theta = 2.9^\circ$. Here $\Omega_{\mathbf{k}}$ is positive definite and fluctuates in sync with $\text{Tr } g_{\mathbf{k}}$. A measure of the deviation from ideal quantum geometry [58, 59] is $T = \frac{1}{2\pi} \int d^2 \mathbf{k} \text{Tr } g_{\mathbf{k}} - \mathcal{C}$, which is bounded by $T \geq 0$ (i.e., the trace inequality). The θ dependence of T is plotted in Fig. 1(b), which is minimum (~ 0.1) at the magic angle $\theta_m = 2.9^\circ$. The nearly saturated bound $T \geq 0$ at θ_m implies a connection with 0LL, which has $T = 0$.

LL representation.— We apply two unitary transformations to H to find a representation of Bloch states in terms of LL wavefunctions. The first unitary transformation is to make the threefold rotational symmetry apparent [69],

$$H_1 = U_0^\dagger(\mathbf{r}) H U_0(\mathbf{r}),$$

$$U_0(\mathbf{r}) = \begin{pmatrix} e^{i\kappa_+ \cdot \mathbf{r}} & 0 \\ 0 & e^{i\kappa_- \cdot \mathbf{r}} \end{pmatrix}, \quad (3)$$

$$H_1 = -\frac{\hbar^2 \hat{\mathbf{k}}^2}{2m^*} \sigma_0 + \mathbf{\Delta}(\mathbf{r}) \cdot \boldsymbol{\sigma} + \Delta_0(\mathbf{r}) \sigma_0,$$

where σ_0 is identity matrix and $\boldsymbol{\sigma}$ are Pauli matrices.

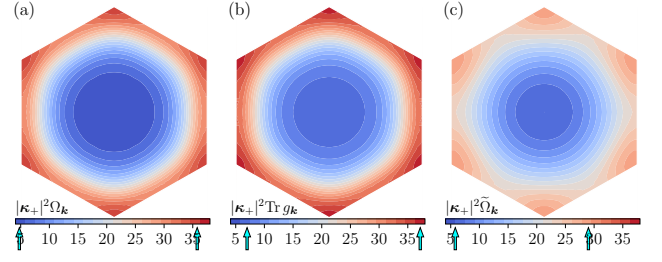


FIG. 2. (a) $\Omega_{\mathbf{k}}$ and (b) $\text{Tr } g_{\mathbf{k}}$ for $\varphi_{1,\mathbf{k}}(\mathbf{r})$ in the moiré Brillouin zone. (c) $\tilde{\Omega}_{\mathbf{k}}$ (identical to $\text{Tr } \tilde{g}_{\mathbf{k}}$ for $\Theta_{\mathbf{k}}(\mathbf{r})$). The arrows indicate the data range in each plot. θ is 2.9° .

The scalar potential $\Delta_0(\mathbf{r})$ and the layer pseudospin field $\mathbf{\Delta}(\mathbf{r})$ are defined as

$$\Delta_0(\mathbf{r}) = \frac{\Delta_+(\mathbf{r}) + \Delta_-(\mathbf{r})}{2},$$

$$\mathbf{\Delta}(\mathbf{r}) = [\text{Re } \tilde{\Delta}_t^\dagger(\mathbf{r}), \text{Im } \tilde{\Delta}_t^\dagger(\mathbf{r}), \frac{\Delta_+(\mathbf{r}) - \Delta_-(\mathbf{r})}{2}], \quad (4)$$

$$\tilde{\Delta}_t^\dagger(\mathbf{r}) = e^{i(\kappa_+ - \kappa_-) \cdot \mathbf{r}} \Delta_t^\dagger(\mathbf{r}).$$

We further define a unit vector $\mathbf{n}(\mathbf{r}) = \mathbf{\Delta}(\mathbf{r}) / |\mathbf{\Delta}(\mathbf{r})|$, which forms a skyrmion lattice as characterized by the winding number [16, 70],

$$N_w = \frac{1}{2\pi} \int_{\mathcal{A}_0} d\mathbf{r} b_z = -1, \quad (5)$$

Here \mathcal{A}_0 is the area expanded by a moiré unit cell and $b_z = \frac{1}{2} \mathbf{n} \cdot (\partial_x \mathbf{n} \times \partial_y \mathbf{n})$.

We construct another unitary matrix $U(\mathbf{r})$ to rotate the layer pseudospin to the local frame of $\mathbf{\Delta}(\mathbf{r})$,

$$U^\dagger(\mathbf{r}) [\mathbf{\Delta}(\mathbf{r}) \cdot \boldsymbol{\sigma}] U(\mathbf{r}) = |\mathbf{\Delta}(\mathbf{r})| \sigma_z. \quad (6)$$

Here $U(\mathbf{r})$ can be parametrized using the polar angle $\vartheta(\mathbf{r})$ and azimuthal angle $\phi(\mathbf{r})$ of $\mathbf{n}(\mathbf{r})$,

$$U(\mathbf{r}) = (\boldsymbol{\chi}^{(+)}(\mathbf{r}), \boldsymbol{\chi}^{(-)}(\mathbf{r})),$$

$$\boldsymbol{\chi}^{(+)}(\mathbf{r}) = e^{i\lambda_+(\mathbf{r})} \left[\cos \frac{\vartheta(\mathbf{r})}{2}, e^{i\phi(\mathbf{r})} \sin \frac{\vartheta(\mathbf{r})}{2} \right]^T, \quad (7)$$

$$\boldsymbol{\chi}^{(-)}(\mathbf{r}) = e^{i\lambda_-(\mathbf{r})} \left[e^{-i\phi(\mathbf{r})} \sin \frac{\vartheta(\mathbf{r})}{2}, -\cos \frac{\vartheta(\mathbf{r})}{2} \right]^T,$$

where $e^{i\lambda_{\pm}(\mathbf{r})}$ represent arbitrary phases. $\boldsymbol{\chi}^{(+)}$ and $\boldsymbol{\chi}^{(-)}$ are spinors that align and antialign with $\mathbf{\Delta}$, respectively.

The nonzero winding number N_w poses an obstruction in choosing $e^{i\lambda_{\pm}(\mathbf{r})}$ such that $U(\mathbf{r})$ is spatially continuous and periodic. However, $U(\mathbf{r})$ can be continuous but quasiperiodic. This motivates us to express $U(\mathbf{r})$ using LL wavefunctions,

$$\boldsymbol{\chi}^{(+)}(\mathbf{r}) = \{\alpha(\mathbf{r}) \Psi_{0,\kappa_-}^{(+)}(\mathbf{r}), \beta(\mathbf{r}) \Psi_{0,\kappa_+}^{(+)}(\mathbf{r})\}^T,$$

$$\boldsymbol{\chi}^{(-)}(\mathbf{r}) = \{\beta^*(\mathbf{r}) [\Psi_{0,\kappa_+}^{(+)}(\mathbf{r})]^*, -\alpha^*(\mathbf{r}) [\Psi_{0,\kappa_-}^{(+)}(\mathbf{r})]^*\}^T. \quad (8)$$

We use $\Psi_{n,\mathbf{k}}^{(\pm)}(\mathbf{r})$ to denote electron magnetic Bloch wavefunction of the n th LL at momentum \mathbf{k} in magnetic field along $\pm\hat{z}$ direction. The 0LL wavefunction $\Psi_{0,\mathbf{k}}^{(+)}(\mathbf{r})$ employed in Eq. (8) has the following expression,

$$\Psi_{0,\mathbf{k}}^{(-)}(\mathbf{r}) = \frac{1}{S_{\mathbf{k}}\ell} \sigma(z + iz_{\mathbf{k}}\ell^2) e^{-\frac{1}{4}|z_{\mathbf{k}}|^2\ell^2 - \frac{1}{4}|z|^2\ell^{-2} + \frac{i}{2}z_{\mathbf{k}}^*z}, \quad (9)$$

$$\Psi_{0,\mathbf{k}}^{(+)}(\mathbf{r}) = [\Psi_{0,-\mathbf{k}}^{(-)}(\mathbf{r})]^*,$$

where $\sigma(z)$ is the modified Weierstrass sigma function [71], $z = x + iy$, $z_{\mathbf{k}} = k_x + ik_y$, $S_{\mathbf{k}}$ is a normalization factor, and $\ell = \sqrt{\mathcal{A}_0/(2\pi)}$.

One specific solution of $\alpha(\mathbf{r})$ and $\beta(\mathbf{r})$ obtained by comparing Eqs. (7) and (8) is,

$$\alpha(\mathbf{r}) = \frac{e^{-i\zeta(\mathbf{r})/2}}{|\Psi_{0,\kappa_-}^{(+)}(\mathbf{r})|} \sqrt{\frac{1+n_z(\mathbf{r})}{2}},$$

$$\beta(\mathbf{r}) = \frac{e^{i\zeta(\mathbf{r})/2}}{|\Psi_{0,\kappa_+}^{(+)}(\mathbf{r})|} \sqrt{\frac{1-n_z(\mathbf{r})}{2}}, \quad (10)$$

$$\zeta(\mathbf{r}) = \text{Arg}\left\{\frac{n_x(\mathbf{r}) + in_y(\mathbf{r})}{[\Psi_{0,\kappa_-}^{(+)}(\mathbf{r})]^* \Psi_{0,\kappa_+}^{(+)}(\mathbf{r})}\right\}.$$

Here n_j is the j component of \mathbf{n} . Because the zeros of $|\Psi_{0,\kappa_{\mp}}^{(+)}(\mathbf{r})|$ and $[\Psi_{0,\kappa_-}^{(+)}(\mathbf{r})]^* \Psi_{0,\kappa_+}^{(+)}(\mathbf{r})$ are exactly cancelled, respectively, by those of $\sqrt{1 \pm n_z(\mathbf{r})}$ and $n_x(\mathbf{r}) + in_y(\mathbf{r})$, $\alpha(\mathbf{r})$ and $\beta(\mathbf{r})$ are periodic functions without singularity.

We now apply $U(\mathbf{r})$ to H_1 ,

$$H_2 = U^\dagger(\mathbf{r})H_1U(\mathbf{r})$$

$$= -\frac{\hbar^2}{2m^*} \begin{pmatrix} (\hat{\mathbf{k}} + \mathbf{A}_{11})^2 & \hat{\mathbf{k}}\mathbf{A}_{12} + \mathbf{A}_{12}\hat{\mathbf{k}} \\ \hat{\mathbf{k}}\mathbf{A}_{21} + \mathbf{A}_{21}\hat{\mathbf{k}} & (\hat{\mathbf{k}} + \mathbf{A}_{22})^2 \end{pmatrix} \quad (11)$$

$$+ |\mathbf{\Delta}(\mathbf{r})|\sigma_z + [\Delta_0(\mathbf{r}) - D(\mathbf{r})]\sigma_0,$$

where $\mathbf{A} = -iU^\dagger(\mathbf{r})\nabla U(\mathbf{r})$ is a non-Abelian gauge field and $D(\mathbf{r}) = \frac{\hbar^2}{2m^*}|\mathbf{A}_{12}|^2$ [17, 39]. The field \mathbf{A}_{ii} generates an effective magnetic field $B_i = \nabla \times \mathbf{A}_{ii}$ with $B_1 = +b_z$ and $B_2 = -b_z$. The flux of B_1 (B_2) over \mathcal{A}_0 is exactly a negative (positive) magnetic flux quantum, according to Eq. (5). Therefore, Bloch state $\Phi_{m,\mathbf{k}}(\mathbf{r})$ of Hamiltonian H_2 for the m th band at momentum \mathbf{k} can be expanded in terms of the magnetic Bloch state $\Psi_{n,\mathbf{k}}^{(\pm)}(\mathbf{r})$,

$$\Phi_{m,\mathbf{k}}(\mathbf{r}) = \sum_n [c_{m,n,\mathbf{k}}^{(+)} \Psi_{n,\mathbf{k}}^{(-)}(\mathbf{r}), c_{m,n,\mathbf{k}}^{(-)} \Psi_{n,\mathbf{k}}^{(+)}(\mathbf{r})]^T, \quad (12)$$

where $c_{m,n,\mathbf{k}}^{(\pm)}$ are expansion coefficients.

The Bloch state $\varphi_{m,\mathbf{k}}(\mathbf{r})$ of the original Hamiltonian H is related to $\Phi_{m,\mathbf{k}}(\mathbf{r})$ by unitary transformations,

$$\varphi_{m,\mathbf{k}}(\mathbf{r}) = U_0(\mathbf{r})U(\mathbf{r})\Phi_{m,\mathbf{k}}(\mathbf{r})$$

$$= \sum_n \sum_{s=\pm} c_{m,n,\mathbf{k}}^{(s)} \psi_{n,\mathbf{k}}^{(s)}(\mathbf{r}), \quad (13)$$

where $\psi_{n,\mathbf{k}}^{(\pm)}(\mathbf{r})$ are a set of orthonormal and complete Bloch bases defined by,

$$\psi_{n,\mathbf{k}}^{(+)}(\mathbf{r}) = U_0(\mathbf{r})\chi^{(+)}(\mathbf{r})\Psi_{n,\mathbf{k}}^{(-)}(\mathbf{r}), \quad (14)$$

$$\psi_{n,\mathbf{k}}^{(-)}(\mathbf{r}) = U_0(\mathbf{r})\chi^{(-)}(\mathbf{r})\Psi_{n,\mathbf{k}}^{(+)}(\mathbf{r}),$$

which are derived from the LL wavefunction $\Psi_{n,\mathbf{k}}^{(-s)}$ dressed by the spinor $U_0(\mathbf{r})\chi^{(s)}$. Because $\chi^{(s)}$ and $\Psi_{n,\mathbf{k}}^{(-s)}$ are magnetic Bloch states under opposite magnetic fields, $\psi_{n,\mathbf{k}}^{(\pm)}$ satisfy Bloch's theorem. Notably, $\psi_{n,\mathbf{k}}^{(\pm)}$ have the same *uniform* quantum geometric tensor as that of $\Psi_{n,\mathbf{k}}^{(\pm)}$, since the spinor $U_0(\mathbf{r})\chi^{(\pm)}(\mathbf{r})$ is \mathbf{k} independent and normalized at every \mathbf{r} . Equations (13) and (14) establish a LL representation of Bloch states.

To characterize the overlap between $\varphi_{m,\mathbf{k}}$ and $\psi_{n,\mathbf{k}}^{(s)}$, we introduce the averaged LL weight,

$$W_{m,n}^{(s)} = \frac{1}{N} \sum_{\mathbf{k}} |c_{m,n,\mathbf{k}}^{(s)}|^2, \quad (15)$$

where N is the number of \mathbf{k} points. We focus on the first moiré band $\varphi_{1,\mathbf{k}}$, which has a dominant contribution from $\psi_{n,\mathbf{k}}^{(+)}$, since the spinor part of $\psi_{n,\mathbf{k}}^{(+)}$ locally follows the skyrmion field $\mathbf{\Delta}(\mathbf{r})$. We numerically find that the weight $W_{1,0}^{(+)}$ on the dressed 0LL wavefunction $\psi_{0,\mathbf{k}}^{(+)}$ is sizable (> 0.6) over a range of twist angle $\theta \in (2.5^\circ, 4.5^\circ)$, as shown in Fig. 1(c). However, $W_{1,0}^{(+)}$ is noticeably below 1 even at θ_m , because the nonuniform quantum geometry of $\varphi_{1,\mathbf{k}}$ is not captured by $\psi_{0,\mathbf{k}}^{(+)}$.

Variational mapping.— To further optimize the weight on the 0LL, we generalize $\psi_{0,\mathbf{k}}^{(+)}$ to $\Theta_{\mathbf{k}}(\mathbf{r})$,

$$\Theta_{\mathbf{k}}(\mathbf{r}) = \mathcal{N}_{\mathbf{k}}U_0(\mathbf{r})\mathcal{B}(\mathbf{r})\Psi_{0,\mathbf{k}}^{(-)}(\mathbf{r}), \quad (16)$$

where $\mathcal{B}(\mathbf{r}) = [\mathcal{B}_1(\mathbf{r}), \mathcal{B}_2(\mathbf{r})]^T$ has two components and $\mathcal{N}_{\mathbf{k}}$ is a normalization factor. Here $\mathcal{B}(\mathbf{r})$ is not required to be normalized, but $\Theta_{\mathbf{k}}(\mathbf{r})$ always has a Chern number $\mathcal{C} = 1$ and an ideal but nonuniform quantum geometry, $\tilde{g}_{\mathbf{k}} = \tilde{\Omega}_{\mathbf{k}}\mathbb{1}/2$, where $\tilde{g}_{\mathbf{k}}$ ($\tilde{\Omega}_{\mathbf{k}}$) is the quantum metric (Berry curvature) of $\Theta_{\mathbf{k}}(\mathbf{r})$ [59].

We define a new weight \tilde{W} as

$$\tilde{W} = \frac{1}{N} \sum_{\mathbf{k}} |\tilde{c}_{\mathbf{k}}|^2, \quad (17)$$

where $\tilde{c}_{\mathbf{k}} = \langle \varphi_{1,\mathbf{k}} | \Theta_{\mathbf{k}} \rangle$. We maximize \tilde{W} using a variational approach. Taking $\chi^{(+)}(\mathbf{r})$ as an initial ansatz for $\mathcal{B}(\mathbf{r})$, we update $\mathcal{B}(\mathbf{r})$ step-by-step using the gradient ascend method until convergence,

$$\text{Re}[\mathcal{B}_i(\mathbf{r})] \rightarrow \text{Re}[\mathcal{B}_i(\mathbf{r})] + \xi \frac{\delta \tilde{W}}{\delta \text{Re}[\mathcal{B}_i(\mathbf{r})]}, \quad (18)$$

$$\text{Im}[\mathcal{B}_i(\mathbf{r})] \rightarrow \text{Im}[\mathcal{B}_i(\mathbf{r})] + \xi \frac{\delta \tilde{W}}{\delta \text{Im}[\mathcal{B}_i(\mathbf{r})]},$$

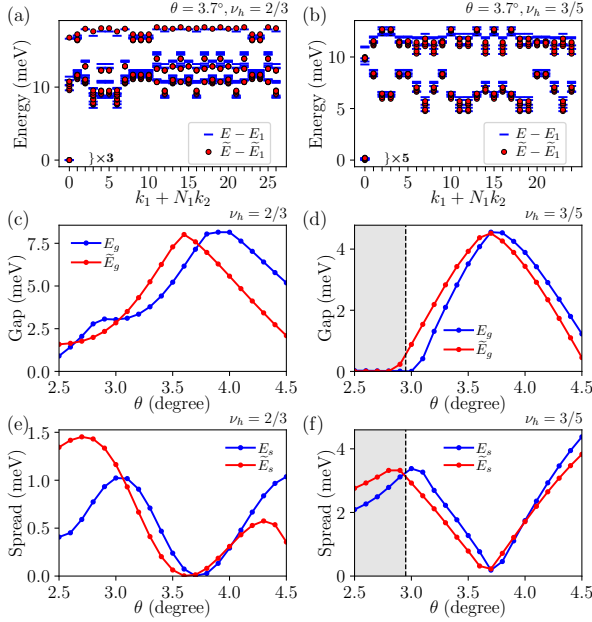


FIG. 3. (a), (b) ED spectra of the original model (blue lines) and variational model (red dots) at $\nu_h = 2/3$ and $3/5$ for $\theta = 3.7^\circ$. Clusters with 27 (25) unit cells are used for $\nu_h = 2/3$ ($3/5$). (c)-(f) Energy gap E_g and spread E_s as functions of θ at $\nu_h = 2/3$ and $3/5$. Blue (red) lines present results from the original (variational) model. The FCIs are absent in the gray regions of (d) and (f), where E_g is zero.

where ξ is a positive parameter.

The maximized \widetilde{W} as a function of θ is shown in Fig. 1(c), which has a significant increase compared to $W_{1,0}^{(+)}$ particularly around θ_m . For $\theta \in (2.5^\circ, 3.7^\circ)$, \widetilde{W} exceeds 0.9 and achieves a maximum of 0.95 at θ_m . The momentum dependence of $|\widetilde{c}_{\mathbf{k}}|$ at θ_m is shown in Fig. 1(d), which is larger than 0.94 for every \mathbf{k} and reaches nearly 1 at the γ point, indicating a high overlap between $\varphi_{1,\mathbf{k}}$ and $\Theta_{\mathbf{k}}$. The spatial variation of $|\mathcal{B}(\mathbf{r})|$ is shown in Fig. 1(e), where the maximal positions form an effective honeycomb lattice, consistent with the density distribution in the first band [31]. Moreover, the quantum geometry fluctuation in $\varphi_{1,\mathbf{k}}(\mathbf{r})$ is qualitatively captured by $\Theta_{\mathbf{k}}(\mathbf{r})$, as illustrated in Fig. 2.

FCIs.— Bloch states of $\Theta_{\mathbf{k}}(\mathbf{r})$ enable construction of trial wavefunction for FCIs [58, 59],

$$\Phi_F = \Psi_F \prod_i U_0(\mathbf{r}_i) \mathcal{B}(\mathbf{r}_i), \quad (19)$$

where \mathbf{r}_i is the position of the i th electron and Ψ_F represents the fractional quantum Hall states (or composite Fermi liquid states) in the OLL. The high overlap between $\varphi_{1,\mathbf{k}}$ and $\Theta_{\mathbf{k}}(\mathbf{r})$ provides a rational explanation for FCIs observed in $t\text{MoTe}_2$.

We study a many-body Hamiltonian given by,

$$\begin{aligned} \hat{H} &= \hat{H}_0 + \hat{H}_{int}, \\ \hat{H}_0 &= \sum_{\mathbf{k}} (-\mathcal{E}_{\mathbf{k}}) b_{\mathbf{k}}^\dagger b_{\mathbf{k}}, \\ \hat{H}_{int} &= \sum_{\mathbf{k}_1 \mathbf{k}_2 \mathbf{k}_3 \mathbf{k}_4} V_{\mathbf{k}_1 \mathbf{k}_2 \mathbf{k}_3 \mathbf{k}_4} b_{\mathbf{k}_1}^\dagger b_{\mathbf{k}_2}^\dagger b_{\mathbf{k}_3} b_{\mathbf{k}_4}, \end{aligned} \quad (20)$$

where we only keep states in the first moiré band at $+K$ valley assuming spontaneous valley polarization, $b_{\mathbf{k}}^\dagger$ ($b_{\mathbf{k}}$) is the creation (annihilation) operator in the *hole* basis, and $-\mathcal{E}_{\mathbf{k}}$ is the hole single-particle energy. The interaction matrix element $V_{\mathbf{k}_1 \mathbf{k}_2 \mathbf{k}_3 \mathbf{k}_4}$ is

$$\begin{aligned} V_{\mathbf{k}_1 \mathbf{k}_2 \mathbf{k}_3 \mathbf{k}_4} &= \frac{1}{2\mathcal{A}} \sum_{\mathbf{q}} V_{\mathbf{q}} M_{\mathbf{k}_1 \mathbf{k}_4}(\mathbf{q}) M_{\mathbf{k}_2 \mathbf{k}_3}(-\mathbf{q}), \\ M_{\mathbf{k} \mathbf{k}'}(\mathbf{q}) &= \int d\mathbf{r} e^{i\mathbf{q} \cdot \mathbf{r}} [f_{\mathbf{k}}(\mathbf{r})]^* f_{\mathbf{k}'}(\mathbf{r}), \end{aligned} \quad (21)$$

where \mathcal{A} is the system area, $V_{\mathbf{q}} = 2\pi e^2 \tanh|\mathbf{q}d|/(\epsilon|\mathbf{q}|)$ is gate screened Coulomb interaction, d is the gate-to-sample distance, and ϵ is the dielectric constant. We set $d = 100$ nm and $\epsilon = 5$. In $M_{\mathbf{k} \mathbf{k}'}(\mathbf{q})$, $f_{\mathbf{k}}(\mathbf{r})$ is $[\varphi_{\mathbf{k},1}(\mathbf{r})]^*$ or $[\Theta_{\mathbf{k}}(\mathbf{r})]^*$, corresponding to the original model and variational model, respectively.

We compare ED spectra of the above two models at $\theta = 3.7^\circ$ in Fig. 3(a) [3(b)] for $\nu_h = 2/3$ ($3/5$), which are obtained using clusters with 27 (25) unit cells. The three (five) quasi-degenerate ground states in the zero momentum sector indicate the presence of the FCIs for both models at $\nu_h = 2/3$ ($3/5$) [4, 25, 34]. Moreover, the excited-state spectra of the original model are approximately reproduced by those of the variational model, as shown in Figs. 3(a) and 3(b).

Figure 3 also plots the charge-neutral gap $E_g = E_4 - E_3$ ($E_6 - E_5$) and ground-state energy spread $E_s = E_3 - E_1$ ($E_5 - E_1$) as functions of θ for $\nu_h = 2/3$ ($3/5$), where E_n is the n th lowest energy in the ED spectra. At $\nu_h = 2/3$, E_g is maximum at $\theta = 3.9^\circ$ (3.6°) in the original (variational) model and is finite for $\theta \in (2.5^\circ, 4.5^\circ)$, indicating a robust FCI phase; E_s is vanishingly small around $\theta = 3.7^\circ$ in both models. The two models also compare quantitatively well at $\nu_h = 3/5$ and share the following features, (1) E_g is maximum and E_s is minimum at $\theta = 3.7^\circ$; (2) E_g is finite only for $\theta \gtrsim 3^\circ$, indicating a narrower range of FCI phase than $\nu_h = 2/3$. We note that the strongest FCI measured by the maximum E_g or minimum E_s do not occur at θ_m . This can be attributed to the spatial variation of $|\mathcal{B}(\mathbf{r})|$, which is strong at θ_m but weakens as θ increases. On the other hand, the decrease of E_g at large θ is due to the increased single-particle bandwidth.

Discussion.— In summary, the variational wavefunction $\Theta_{\mathbf{k}}(\mathbf{r})$ successfully captures both the single-particle and many-body physics. We expect applications of our theory in several directions. First, the wavefunction Φ_F

in Eq. (19) can be generalized to excited states of fractionalized quasihole and quasielectron [72]. After $\Theta_{\mathbf{k}}(\mathbf{r})$ is determined using the variational approach, energies of Φ_F and related excited states can be calculated using the Monte Carlo method. The energy to create free quasiparticle-quasihole pairs can then be estimated, which should determine the activation gap in transport in the clean limit [73]. Second, the variational mapping between higher-energy moiré bands and higher-index LL can be performed using our approach combined with the recently proposed theory of generalized LL [74]. Several theoretical works reported non-Abelian fractional states at half-filling of the second moiré band [43–46], whose connection to the first LL can be worked out. Finally, FCIs at zero magnetic field have also been observed in a rhombohedral pentalayer graphene–hBN moiré superlattice [12] and theoretically proposed in various models [75–78]. The extension of our theory to systems beyond $t\text{MoTe}_2$ is conceivable.

Acknowledgments.— We thank Jie Wang and Zhao Liu for valuable discussions. This work is supported by National Key Research and Development Program of China (Grants No. 2021YFA1401300 and No. 2022YFA1402401), National Natural Science Foundation of China (Grant No. 12274333), and start-up funding of Wuhan University. The numerical calculations in this paper have been performed on the supercomputing system in the Supercomputing Center of Wuhan University.

* wufcheng@whu.edu.cn

- [1] E. Tang, J.-W. Mei, and X.-G. Wen, High-temperature fractional quantum Hall states, *Phys. Rev. Lett.* **106**, 236802 (2011).
- [2] K. Sun, Z. Gu, H. Katsura, and S. Das Sarma, Nearly flatbands with nontrivial topology, *Phys. Rev. Lett.* **106**, 236803 (2011).
- [3] T. Neupert, L. Santos, C. Chamon, and C. Mudry, Fractional quantum Hall states at zero magnetic field, *Phys. Rev. Lett.* **106**, 236804 (2011).
- [4] N. Regnault and B. A. Bernevig, Fractional Chern insulator, *Phys. Rev. X* **1**, 021014 (2011).
- [5] D. N. Sheng, Z.-C. Gu, K. Sun, and L. Sheng, Fractional quantum hall effect in the absence of landau levels, *Nature Communications* **2**, 389 (2011).
- [6] E. M. Spanton, A. A. Zibrov, H. Zhou, T. Taniguchi, K. Watanabe, M. P. Zaletel, and A. F. Young, Observation of fractional Chern insulators in a van der Waals heterostructure, *Science* **360**, 62 (2018).
- [7] Y. Xie, A. T. Pierce, J. M. Park, D. E. Parker, E. Khalaf, P. Ledwith, Y. Cao, S. H. Lee, S. Chen, P. R. Forrester, K. Watanabe, T. Taniguchi, A. Vishwanath, P. Jarillo-Herrero, and A. Yacoby, Fractional Chern insulators in magic-angle twisted bilayer graphene, *Nature* **600**, 439 (2021).
- [8] J. Cai, E. Anderson, C. Wang, X. Zhang, X. Liu, W. Holtzmann, Y. Zhang, F. Fan, T. Taniguchi, K. Watanabe, Y. Ran, T. Cao, L. Fu, D. Xiao, W. Yao, and X. Xu, Signatures of fractional quantum anomalous Hall states in twisted MoTe_2 , *Nature* **622**, 63 (2023).
- [9] Y. Zeng, Z. Xia, K. Kang, J. Zhu, P. Knüppel, C. Vaswani, K. Watanabe, T. Taniguchi, K. F. Mak, and J. Shan, Thermodynamic evidence of fractional Chern insulator in moiré MoTe_2 , *Nature* **622**, 69 (2023).
- [10] H. Park, J. Cai, E. Anderson, Y. Zhang, J. Zhu, X. Liu, C. Wang, W. Holtzmann, C. Hu, Z. Liu, T. Taniguchi, K. Watanabe, J.-H. Chu, T. Cao, L. Fu, W. Yao, C.-Z. Chang, D. Cobden, D. Xiao, and X. Xu, Observation of fractionally quantized anomalous Hall effect, *Nature* **622**, 74 (2023).
- [11] F. Xu, Z. Sun, T. Jia, C. Liu, C. Xu, C. Li, Y. Gu, K. Watanabe, T. Taniguchi, B. Tong, J. Jia, Z. Shi, S. Jiang, Y. Zhang, X. Liu, and T. Li, Observation of integer and fractional quantum anomalous Hall effects in twisted bilayer MoTe_2 , *Phys. Rev. X* **13**, 031037 (2023).
- [12] Z. Lu, T. Han, Y. Yao, A. P. Reddy, J. Yang, J. Seo, K. Watanabe, T. Taniguchi, L. Fu, and L. Ju, Fractional quantum anomalous Hall effect in multilayer graphene, *Nature* **626**, 759 (2024).
- [13] Z. Ji, H. Park, M. E. Barber, C. Hu, K. Watanabe, T. Taniguchi, J.-H. Chu, X. Xu, and Z.-X. Shen, Local probe of bulk and edge states in a fractional Chern insulator, [arXiv:2404.07157](https://arxiv.org/abs/2404.07157).
- [14] E. Redekop, C. Zhang, H. Park, J. Cai, E. Anderson, O. Sheekey, T. Arp, G. Babikyan, S. Salters, K. Watanabe, T. Taniguchi, X. Xu, and A. F. Young, Direct magnetic imaging of fractional Chern insulators in twisted MoTe_2 with a superconducting sensor, [arXiv:2405.10269](https://arxiv.org/abs/2405.10269).
- [15] K. Kang, B. Shen, Y. Qiu, Y. Zeng, Z. Xia, K. Watanabe, T. Taniguchi, J. Shan, and K. F. Mak, Evidence of the fractional quantum spin Hall effect in moiré MoTe_2 , *Nature* **628**, 522 (2024).
- [16] F. Wu, T. Lovorn, E. Tutuc, I. Martin, and A. H. MacDonald, Topological insulators in twisted transition metal dichalcogenide homobilayers, *Phys. Rev. Lett.* **122**, 086402 (2019).
- [17] H. Yu, M. Chen, and W. Yao, Giant magnetic field from moiré induced Berry phase in homobilayer semiconductors, *National Science Review* **7**, 12 (2019).
- [18] T. Devakul, V. Crépel, Y. Zhang, and L. Fu, Magic in twisted transition metal dichalcogenide bilayers, *Nature Communications* **12**, 6730 (2021).
- [19] H. Li, U. Kumar, K. Sun, and S.-Z. Lin, Spontaneous fractional Chern insulators in transition metal dichalcogenide moiré superlattices, *Phys. Rev. Res.* **3**, L032070 (2021).
- [20] V. Crépel and L. Fu, Anomalous Hall metal and fractional Chern insulator in twisted transition metal dichalcogenides, *Phys. Rev. B* **107**, L201109 (2023).
- [21] N. Morales-Durán, J. Wang, G. R. Schleder, M. Angeli, Z. Zhu, E. Kaxiras, C. Repellin, and J. Cano, Pressure-enhanced fractional Chern insulators along a magic line in moiré transition metal dichalcogenides, *Phys. Rev. Res.* **5**, L032022 (2023).
- [22] H. Goldman, A. P. Reddy, N. Paul, and L. Fu, Zero-field composite Fermi liquid in twisted semiconductor bilayers, *Phys. Rev. Lett.* **131**, 136501 (2023).
- [23] J. Dong, J. Wang, P. J. Ledwith, A. Vishwanath, and D. E. Parker, Composite fermi liquid at zero magnetic field in twisted MoTe_2 , *Phys. Rev. Lett.* **131**, 136502 (2023).

- [24] A. P. Reddy and L. Fu, Toward a global phase diagram of the fractional quantum anomalous Hall effect, *Phys. Rev. B* **108**, 245159 (2023).
- [25] A. P. Reddy, F. Alsallom, Y. Zhang, T. Devakul, and L. Fu, Fractional quantum anomalous Hall states in twisted bilayer MoTe₂ and WSe₂, *Phys. Rev. B* **108**, 085117 (2023).
- [26] C. Wang, X.-W. Zhang, X. Liu, Y. He, X. Xu, Y. Ran, T. Cao, and D. Xiao, Fractional Chern insulator in twisted bilayer MoTe₂, *Phys. Rev. Lett.* **132**, 036501 (2024).
- [27] C. Xu, J. Li, Y. Xu, Z. Bi, and Y. Zhang, Maximally localized Wannier functions, interaction models, and fractional quantum anomalous Hall effect in twisted bilayer MoTe₂, *Proceedings of the National Academy of Sciences* **121**, e2316749121 (2024).
- [28] N. Mao, C. Xu, J. Li, T. Bao, P. Liu, Y. Xu, C. Felser, L. Fu, and Y. Zhang, Lattice relaxation, electronic structure and continuum model for twisted bilayer MoTe₂, [arXiv:2311.07533](https://arxiv.org/abs/2311.07533).
- [29] X.-W. Zhang, C. Wang, X. Liu, Y. Fan, T. Cao, and D. Xiao, Polarization-driven band topology evolution in twisted MoTe₂ and WSe₂, *Nature Communications* **15**, 4223 (2024).
- [30] Y. Jia, J. Yu, J. Liu, J. Herzog-Arbeitman, Z. Qi, H. Pi, N. Regnault, H. Weng, B. A. Bernevig, and Q. Wu, Moiré fractional Chern insulators. i. first-principles calculations and continuum models of twisted bilayer MoTe₂, *Phys. Rev. B* **109**, 205121 (2024).
- [31] W.-X. Qiu, B. Li, X.-J. Luo, and F. Wu, Interaction-driven topological phase diagram of twisted bilayer MoTe₂, *Phys. Rev. X* **13**, 041026 (2023).
- [32] B. Li, W.-X. Qiu, and F. Wu, Electrically tuned topology and magnetism in twisted bilayer MoTe₂ at $\nu_h = 1$, *Phys. Rev. B* **109**, L041106 (2024).
- [33] X.-J. Luo, W.-X. Qiu, and F. Wu, Majorana zero modes in twisted transition metal dichalcogenide homobilayers, *Phys. Rev. B* **109**, L041103 (2024).
- [34] J. Yu, J. Herzog-Arbeitman, M. Wang, O. Vafek, B. A. Bernevig, and N. Regnault, Fractional Chern insulators versus nonmagnetic states in twisted bilayer MoTe₂, *Phys. Rev. B* **109**, 045147 (2024).
- [35] A. Abouelkomsan, A. P. Reddy, L. Fu, and E. J. Bergholtz, Band mixing in the quantum anomalous Hall regime of twisted semiconductor bilayers, *Phys. Rev. B* **109**, L121107 (2024).
- [36] X.-Y. Song, Y.-H. Zhang, and T. Senthil, Phase transitions out of quantum Hall states in moiré materials, *Phys. Rev. B* **109**, 085143 (2024).
- [37] F.-R. Fan, C. Xiao, and W. Yao, Orbital Chern insulator at $\nu = -2$ in twisted MoTe₂, *Phys. Rev. B* **109**, L041403 (2024).
- [38] X. Liu, Y. He, C. Wang, X.-W. Zhang, T. Cao, and D. Xiao, Gate-tunable antiferromagnetic Chern insulator in twisted bilayer transition metal dichalcogenides, *Phys. Rev. Lett.* **132**, 146401 (2024).
- [39] N. Morales-Durán, N. Wei, J. Shi, and A. H. MacDonald, Magic angles and fractional Chern insulators in twisted homobilayer transition metal dichalcogenides, *Phys. Rev. Lett.* **132**, 096602 (2024).
- [40] J. Shi, N. Morales-Durán, E. Khalaf, and A. H. MacDonald, Adiabatic approximation and Aharonov-Casher bands in twisted homobilayer TMDs, [arXiv:2404.13455](https://arxiv.org/abs/2404.13455).
- [41] V. Crépel, N. Regnault, and R. Queiroz, Chiral limit and origin of topological flat bands in twisted transition metal dichalcogenide homobilayers, *Communications Physics* **7**, 146 (2024).
- [42] T. Wang, M. Wang, W. Kim, S. G. Louie, L. Fu, and M. P. Zaletel, Topology, magnetism and charge order in twisted MoTe₂ at higher integer hole fillings, [arXiv:2312.12531](https://arxiv.org/abs/2312.12531).
- [43] A. P. Reddy, N. Paul, A. Abouelkomsan, and L. Fu, Non-abelian fractionalization in topological minibands, [arXiv:2403.00059](https://arxiv.org/abs/2403.00059).
- [44] C. Xu, N. Mao, T. Zeng, and Y. Zhang, Multiple Chern bands in twisted MoTe₂ and possible non-abelian states, [arXiv:2403.17003](https://arxiv.org/abs/2403.17003).
- [45] C.-E. Ahn, W. Lee, K. Yananose, Y. Kim, and G. Y. Cho, First Landau level physics in second Moiré band of 2.1° twisted bilayer MoTe₂, [arXiv:2403.19155](https://arxiv.org/abs/2403.19155).
- [46] C. Wang, X.-W. Zhang, X. Liu, J. Wang, T. Cao, and D. Xiao, Higher Landau-level analogues and signatures of non-abelian states in twisted bilayer MoTe₂, [arXiv:2404.05697](https://arxiv.org/abs/2404.05697).
- [47] Y.-H. Zhang, Non-abelian and abelian descendants of vortex spin liquid: fractional quantum spin Hall effect in twisted MoTe₂, [arXiv:2403.12126](https://arxiv.org/abs/2403.12126).
- [48] C.-M. Jian, M. Cheng, and C. Xu, Minimal fractional topological insulator in half-filled conjugate moiré Chern bands, [arXiv:2403.07054](https://arxiv.org/abs/2403.07054).
- [49] I. S. Villadiago, Halperin states of particles and holes in ideal time reversal invariant pairs of Chern bands and the fractional quantum spin Hall effect in Moiré MoTe₂, [arXiv:2403.12185](https://arxiv.org/abs/2403.12185).
- [50] J. May-Mann, A. Stern, and T. Devakul, Theory of half-integer fractional quantum spin Hall insulator edges, [arXiv:2403.03964](https://arxiv.org/abs/2403.03964).
- [51] M. Wang, X. Wang, and O. Vafek, Interacting phase diagram of twisted bilayer MoTe₂ in magnetic field, [arXiv:2405.14811](https://arxiv.org/abs/2405.14811).
- [52] X.-L. Qi, Generic wave-function description of fractional quantum anomalous Hall states and fractional topological insulators, *Phys. Rev. Lett.* **107**, 126803 (2011).
- [53] Y.-L. Wu, N. Regnault, and B. A. Bernevig, Gauge-fixed Wannier wave functions for fractional topological insulators, *Phys. Rev. B* **86**, 085129 (2012).
- [54] S. A. Parameswaran, R. Roy, and S. L. Sondhi, Fractional quantum Hall physics in topological flat bands, *Comptes Rendus. Physique* **14**, 816 (2013).
- [55] T. S. Jackson, G. Möller, and R. Roy, Geometric stability of topological lattice phases, *Nature Communications* **6**, 8629 (2015).
- [56] M. Claassen, C. H. Lee, R. Thomale, X.-L. Qi, and T. P. Devereaux, Position-momentum duality and fractional quantum Hall effect in chern insulators, *Phys. Rev. Lett.* **114**, 236802 (2015).
- [57] G. Tarnopolsky, A. J. Kruchkov, and A. Vishwanath, Origin of magic angles in twisted bilayer graphene, *Phys. Rev. Lett.* **122**, 106405 (2019).
- [58] P. J. Ledwith, G. Tarnopolsky, E. Khalaf, and A. Vishwanath, Fractional Chern insulator states in twisted bilayer graphene: An analytical approach, *Phys. Rev. Res.* **2**, 023237 (2020).
- [59] J. Wang, J. Cano, A. J. Millis, Z. Liu, and B. Yang, Exact Landau level description of geometry and interaction in a flatband, *Phys. Rev. Lett.* **127**, 246403 (2021).
- [60] J. Wang, Y. Zheng, A. J. Millis, and J. Cano, Chiral approximation to twisted bilayer graphene: Exact intraval-

- ley inversion symmetry, nodal structure, and implications for higher magic angles, *Phys. Rev. Res.* **3**, 023155 (2021).
- [61] T. Ozawa and B. Mera, Relations between topology and the quantum metric for Chern insulators, *Phys. Rev. B* **104**, 045103 (2021).
- [62] B. Mera and T. Ozawa, Kähler geometry and Chern insulators: Relations between topology and the quantum metric, *Phys. Rev. B* **104**, 045104 (2021).
- [63] J. Wang and Z. Liu, Hierarchy of ideal flatbands in chiral twisted multilayer graphene models, *Phys. Rev. Lett.* **128**, 176403 (2022).
- [64] P. J. Ledwith, A. Vishwanath, and E. Khalaf, Family of ideal Chern flatbands with arbitrary Chern number in chiral twisted graphene multilayers, *Phys. Rev. Lett.* **128**, 176404 (2022).
- [65] P. J. Ledwith, A. Vishwanath, and D. E. Parker, Vortexability: A unifying criterion for ideal fractional Chern insulators, *Phys. Rev. B* **108**, 205144 (2023).
- [66] J. Wang, S. Klevtsov, and Z. Liu, Origin of model fractional Chern insulators in all topological ideal flatbands: Explicit color-entangled wave function and exact density algebra, *Phys. Rev. Res.* **5**, 023167 (2023).
- [67] J. Dong, P. J. Ledwith, E. Khalaf, J. Y. Lee, and A. Vishwanath, Many-body ground states from decomposition of ideal higher Chern bands: Applications to chirally twisted graphene multilayers, *Phys. Rev. Res.* **5**, 023166 (2023).
- [68] M. Fujimoto, D. E. Parker, J. Dong, E. Khalaf, A. Vishwanath, and P. Ledwith, Higher vortexability: zero field realization of higher Landau levels, [arXiv:2403.00856](https://arxiv.org/abs/2403.00856).
- [69] X.-J. Luo, M. Wang, and F. Wu, Symmetric Wannier states and tight-binding model for quantum spin Hall bands in AB-stacked MoTe₂/WSe₂, *Phys. Rev. B* **107**, 235127 (2023).
- [70] H. Pan, F. Wu, and S. Das Sarma, Band topology, Hubbard model, Heisenberg model, and Dzyaloshinskii-Moriya interaction in twisted bilayer WSe₂, *Phys. Rev. Res.* **2**, 033087 (2020).
- [71] F. D. M. Haldane, A modular-invariant modified Weierstrass sigma-function as a building block for lowest-Landau-level wavefunctions on the torus, *Journal of Mathematical Physics* **59**, 071901 (2018).
- [72] R. B. Laughlin, Anomalous quantum Hall effect: An incompressible quantum fluid with fractionally charged excitations, *Phys. Rev. Lett.* **50**, 1395 (1983).
- [73] S. Das Sarma and M. Xie, On the zero-field quantization of the anomalous quantum Hall effect in two-dimensional moiré layers, *Phys. Rev. B* **109**, L121104 (2024).
- [74] Z. Liu, B. Mera, M. Fujimoto, T. Ozawa, and J. Wang, Theory of generalized Landau levels and implication for non-abelian states, [arXiv:2405.14479](https://arxiv.org/abs/2405.14479).
- [75] S. A. A. Ghorashi, A. Dunbrack, A. Abouelkomsan, J. Sun, X. Du, and J. Cano, Topological and stacked flat bands in bilayer graphene with a superlattice potential, *Phys. Rev. Lett.* **130**, 196201 (2023).
- [76] X. Wan, S. Sarkar, S.-Z. Lin, and K. Sun, Topological exact flat bands in two-dimensional materials under periodic strain, *Phys. Rev. Lett.* **130**, 216401 (2023).
- [77] Q. Gao, J. Dong, P. Ledwith, D. Parker, and E. Khalaf, Untwisting moiré physics: Almost ideal bands and fractional Chern insulators in periodically strained monolayer graphene, *Phys. Rev. Lett.* **131**, 096401 (2023).
- [78] T. Tan, A. P. Reddy, L. Fu, and T. Devakul, Designing topology and fractionalization in narrow gap semiconductor films via electrostatic engineering, [arXiv:2402.03085](https://arxiv.org/abs/2402.03085).